



Universiteit  
Leiden  
The Netherlands

## **Ab initio molecular dynamics calculations on reactions of molecules with metal surfaces**

Nattino, F.

### **Citation**

Nattino, F. (2015, October 28). *Ab initio molecular dynamics calculations on reactions of molecules with metal surfaces*. Retrieved from <https://hdl.handle.net/1887/35980>

Version: Corrected Publisher's Version

License: [Licence agreement concerning inclusion of doctoral thesis in the Institutional Repository of the University of Leiden](#)

Downloaded from: <https://hdl.handle.net/1887/35980>

**Note:** To cite this publication please use the final published version (if applicable).

Cover Page



Universiteit Leiden



The handle <http://hdl.handle.net/1887/35980> holds various files of this Leiden University dissertation

**Author:** Nattino, Francesco

**Title:** Ab initio molecular dynamics calculations on reactions of molecules with metal surfaces

**Issue Date:** 2015-10-28

## Chapter 3

# Effect of Surface Motion on the Rotational Quadrupole Alignment Parameter of D<sub>2</sub> Reacting on Cu(111)

This chapter is based on:

F. Nattino, C. Díaz, B. Jackson, and G. J. Kroes, Phys. Rev. Lett. **108**, 236104 (2012).

### Abstract

*Ab initio* molecular dynamics (AIMD) calculations using the specific reaction parameter approach to density functional theory are presented for the reaction of D<sub>2</sub> on Cu(111) at high surface temperature ( $T_s = 925$  K). The focus is on the dependence of reaction on the alignment of the molecule's angular momentum relative to the surface. For the two rovibrational states for which measured energy resolved rotational quadrupole alignment parameters are available, and for the energies for which statistically accurate rotational quadrupole alignment parameters could be computed, statistically significant results of our AIMD calculations are that, on average: (i) including the effect of the experimental surface temperature (925 K) in the AIMD simulations leads to decreased rotational quadrupole alignment parameters, and (ii) including this effect leads to increased agree-

ment with experiment.

## 3.1 Introduction

Experiments on the alignment dependence of molecule-surface reactions yield detailed information on the interaction of molecules with surfaces [1–3]. Because the rotational alignment parameter of reacting molecules is connected with the local anisotropy of the potential energy surface (PES), measurements of this parameter in conjunction with theory can lead to the identification of the reaction site [4, 5]. Measurement of this parameter as a function of translational energy may also reveal important mechanistic information on, for instance, the importance of orientational steering for reaction [3].

The sensitivity of the alignment of reacting molecules to the details of the molecule-surface interaction makes experiments addressing this topic ideal for testing electronic structure theories that attempt to model this interaction. Such tests are highly relevant, and pose huge challenges. About 90% of the chemical manufacturing processes used worldwide employ heterogeneous catalysts [6]. However, the best *ab initio* theory that can now be used to map out PESs for elementary molecule-surface reactions, density functional theory (DFT) at the generalized gradient approximation (GGA), non-separable gradient approximation (NGA), meta-GGA or meta-NGA level, can provide reaction barriers with an accuracy of no better than 1.8 kcal/mol for gas phase reactions [7, 8]. Even this accuracy has only recently become available [7, 8], and it is therefore not surprising that quantum dynamics calculations using DFT PESs on the rotational quadrupole alignment parameter of  $H_2$  desorbing from metal surfaces such as Pd(100) [9] and Cu(111) [10, 11] have not yet been able to quantitatively reproduce the experiments.

Dihydrogen-metal surface systems are ideal for testing electronic structure methods as accurate reaction probabilities can be computed within the Born-Oppenheimer (BO) approximation [12]. Making the static surface approximation (neglecting energy transfer involving phonons) should likewise lead to accurate results for low surface temperature ( $T_s$ ) [13]. Taking advantage of this, it was recently shown that specific reaction param-

ter DFT (SRP-DFT) [14] allows a chemically accurate description (to within 1 kcal/mol  $\approx$  43 meV) of experiments on reaction of  $\text{H}_2$  and  $\text{D}_2$  in molecular beams, on the influence of the initial rovibrational state of  $\text{H}_2$  on reaction, and on rotational excitation of  $\text{H}_2$ , in scattering from Cu(111) [10, 11]. However, a quantitative description of experiments on the rotational alignment parameter of  $\text{D}_2$  desorbing from Cu(111) was not yet realized [11].

The failure was attributed to errors in the dynamical model (the Born-Oppenheimer static surface (BOSS) model), noting that the alignment experiments [3] were performed at high  $T_s$ . In the experiments  $\text{D}_2$  was permeated through a copper crystal, and alignment parameters were measured for  $\text{D}_2$  recombinatively desorbed from Cu(111) using linearly polarized laser light and time-of-flight techniques to achieve rovibrational state selectivity and translational energy ( $E$ ) resolution. The use of the permeation technique dictated the use of a high  $T_s$  (925 K). Associative desorption experiments at this  $T_s$  have also been used to derive initial state-selected, degeneracy averaged dissociative chemisorption probabilities  $R_{v,J}(E)$  [15], which are closely related to alignment parameters ( $v$  and  $J$  are the vibrational and rotational quantum numbers of  $\text{D}_2$ , see Section 3.2). Deriving parameters describing  $R_{v,J}(E)$  required the assumption that dissociative chemisorption and associative desorption are related by detailed balance. The experimentalists confirmed the validity of this assumption by showing that sticking probabilities measured in molecular beam experiments at low  $T_s$  (120 K) could be well fitted using the  $R_{v,J}(E)$  derived from associative desorption experiments, if the widths of the  $R_{v,J}(E)$  curves were adjusted on the basis of existing knowledge regarding their dependence on  $T_s$  [15]. The detailed balance assumption is probably also valid for the fully initial state-selected resolved reaction probabilities  $R_{v,J,m_J}$  required for the computation of alignment parameters ( $m_J$  is the magnetic rotational quantum number of  $\text{D}_2$ , see Section 3.2), and theorists have relied on this assumption in previous calculations [9, 11]. However, for  $\text{D}_2 + \text{Cu(111)}$  and  $\text{H}_2$ -metal systems in general, no information is available on how  $T_s$  affects  $R_{v,J,m_J}$ , and thereby the alignment parameter. Here our aim is to resolve this issue for  $\text{D}_2 + \text{Cu(111)}$ .

Using approximate molecule-phonon models, the effect of phonons on reactive scattering has been studied with reduced dimensionality models for  $H_2 + Cu$  [13, 16, 17], and treating all six molecular degrees of freedom for  $H_2 + Pd$  surfaces [18, 19]. DFT calculations on  $H_2 + Cu(111)$  have shown that the molecule-phonon coupling intricately depends on the motion of both first and second layer Cu atoms [20]. This complicated dependence is best handled by a method allowing surface atom motion and computing forces on the fly, such as the *ab initio* molecular dynamics (AIMD) method, which was first used to compute probabilities for molecule-surface reactions by Groß and coworkers [21]. They investigated  $H_2$  dissociation on surfaces with initial  $T_s = 0$  K. By extending the application of AIMD to non-zero initial  $T_s$ , here we show that quantitatively accurate modeling of the alignment parameter of  $D_2$  desorbing from metal surfaces requires incorporation of surface motion in the theory. We show this by demonstrating that including the effect of the high experimental  $T_s$  in the theory yields rotational alignment parameters for  $D_2 + Cu(111)$  that, on average, differ significantly from static surface model results for the two rovibrational  $D_2$  states for which experimental results have been obtained. Including the effect of the high experimental  $T_s$  also significantly improves the overall agreement with experiment. The AIMD results also yield an improved description of the initial state-selected reaction probability for  $D_2 + Cu(111)$ .

## 3.2 Methods

The AIMD calculations were done using the *ab initio* total-energy and molecular dynamics program VASP [22–26]. Individual collisions are modeled through *NVU* simulations keeping the number of atoms  $N$ , the cell size  $V$ , and the total energy  $U$  constant, the approximation of omitting a thermostat being appropriate for the direct scattering problem addressed here. The quasi-classical trajectory (QCT) method was used (meaning that in all cases we impart zero-point energy to  $D_2$ ), with appropriate averaging of the initial molecular coordinates and momenta [10, 11].

To mimic the effect of the high  $T_s$  used in the experiments (925 K), the initial coordinates and velocities of the Cu atoms in the upper 3 layers of the surface were

sampled from 1 ps runs of eight differently initialized (111) surfaces, in which these atoms were allowed to move. The sampling procedure used consisted of initially sampling the displacements and velocities of moving Cu atoms from a classical Boltzmann distribution of atomic harmonic oscillators at  $T_s = 925$  K, performing an equilibration AIMD run, an AIMD run with velocity rescaling to the target temperature, another equilibration run and a run for sampling, for each surface. In the AIMD simulations, the lowest layer of Cu atoms of the four layer (2x2) surface unit cell used was kept fixed, whereas the atoms in the upper 3 layers were allowed to move. In the slab and subsequent  $D_2 + Cu(111)$  simulations, the dimensions of the unit cell parallel to the surface were increased by 1.54% relative to their theoretical 0 K values to describe the experimentally determined expansion of bulk Cu [27,28], based on a theoretical 0 K bulk lattice constant  $a_{3D}$  of 3.68 Å. The procedure used imposed an average  $T_s$  of 912 K on the surfaces, with a standard deviation of 167 K that mimics local variations that can be expected in the kinetic energy of an ensemble of  $N = 12$  moving atoms ( $\sigma_T = T/\sqrt{3N} = 154$  K). This allows us to model the effect of local variations of temperature without having to perform prohibitively expensive simulations involving too large surface unit cells.

The AIMD calculations on  $D_2 + Cu(111)$  used a timestep of 0.5 fs. Reaction is defined to take place if the D-D distance  $r$  becomes larger than 1.6 Å, and additionally it becomes larger than the distance between one D-atom and the closest periodic image of the other D-atom. This definition allows for scattering involving recrossings of the transition state (a minority event). The  $D_2$  is started moving to the surface at a molecule-surface distance  $Z = 6.0$  Å, and is considered as scattered once  $Z$  becomes larger than 6.1 Å.

The details of the DFT calculations (number of layers of the Cu slab, number of k-points, etc.) within the AIMD are mostly identical to those of earlier static surface calculations [10,11]. However, the SRP functional used here (called SRP48) employs an RPBE coefficient of 0.48 instead of the previous value (0.43), to account for technical differences in the k-space integration between VASP ( $\Gamma$ -point included) and the previously used electronic structure code ( $\Gamma$ -point not included when using even numbers of

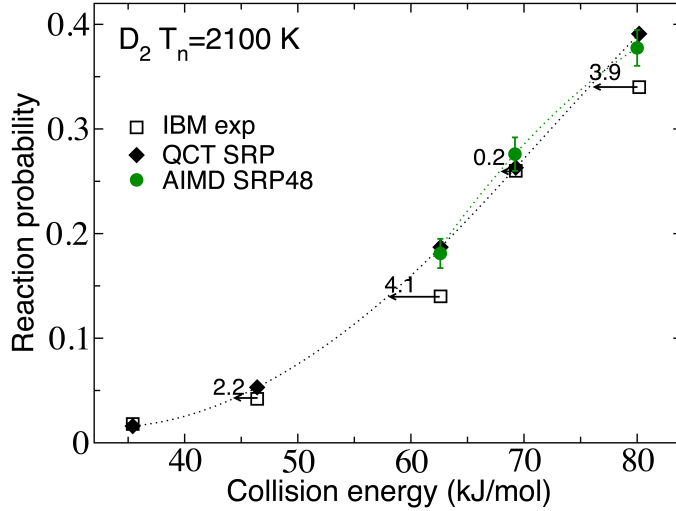


Figure 3.1: Reaction probabilities computed with AIMD are compared with experimental values for  $D_2 + Cu(111)$  [15], and to QCT results employing the BOSS model [10,11]. The experiments used a nozzle temperature of 2100 K. The arrows and the accompanying numbers (in kJ/mol) show the collision energy spacing between the experimental data and the cubic spline interpolated SRP48-DFT reaction probability curve.

k-points) [10,11]. Also, in the SRP48 functional the PW91 functional was replaced by the PBE functional designed to mimic it [29]. SRP48 calculations on  $H_2 + Cu(111)$  for an ideal, 0 K slab reproduce the SRP energies at SRP reaction barrier geometries to within 15 meV. AIMD calculations on  $D_2 + Cu(111)$  using the SRP48 functional and Cu slabs equilibrated at  $T_s = 120$  K reproduced the sticking probability measured at that  $T_s$  for the three translational energies considered to within chemical accuracy (Figure 3.1, 1 kcal/mol  $\approx$  4.2 kJ/mol). This establishes the validity of the SRP48 functional when used with VASP and the present computational parameters.

We have also performed AIMD calculations with VASP in which the surface was kept fixed in an ideal lattice configuration that is appropriate for a 0 K surface, based on the computed 0 K lattice constant and interlayer relaxations of the four-layer slab (AIMDf, where the f stands for fixed lattice). Relative to our earlier QCT-BOSS model [10,11], our AIMDf static surface model shows a number of improvements. The imposition of



artificial symmetry that was used in constructing the SRP PES in the BOSS model (the approximation often made that dihydrogen interacts identically with the fcc and hcp hollow sites) was avoided. The SRP PES used in the QCT-BOSS calculation is affected by small errors incurred in the interpolation procedure used [10, 11]; these admittedly small errors are avoided in the AIMDf calculations. Furthermore the SRP48 0 K lattice constant value (3.68 Å) used in AIMDf agrees better with experiment (3.61 Å) than the RPBE value of 3.71 Å [10, 11] used to construct the SRP PES. We believe that the above improvements made in the AIMDf model explain that the AIMDf results presented in Section 3.3 already agree better with experiment than the QCT-BOSS results.

Assuming detailed balance, the rotational quadrupole alignment parameter for associative desorption was computed using [5]:

$$A_0^{(2)} = \frac{A}{B} = \frac{\sum_{m_J} R_{v,J,m_J}(E) \{3m_J^2 - J(J+1)\} / \{J(J+1)\}}{\sum_{m_J} R_{v,J,m_J}(E)}, \quad (3.1)$$

with the denominator  $B$  being equal to  $(2J+1)R_{v,J}$ , and the quantum numbers referring to the initial state of  $D_2$ .  $A_0^{(2)}$  is positive if the molecule prefers to react with its bond axis parallel to the surface (helicopter rotation,  $|m_J| = J$ ), and negative if the molecule prefers to react end-on (cartwheel rotation,  $m_J = 0$ ), and 0 if reaction is independent of orientation. In all theoretical results shown here, errors and error bars represent 68.3% confidence intervals. Calculations were done for the two  $D_2$  rovibrational states investigated experimentally, at  $E$  values for which statistically accurate AIMD results could be obtained. The AIMD results were based on 3120 (1840) trajectories for the lowest  $E$  investigated for  $v = 1, J = 6$  ( $v = 0, J = 11$ ), and on half these amounts for the other  $E$ 's.

### 3.3 Results and Discussion

For the two states for which energy resolved experimental results are available, the  $A_0^{(2)}$  values computed with AIMD are lower than the AIMD results computed for a fixed

surface at 0 K (AIMDf) for all but one case ( $(v = 1, J = 6)$  at  $E = 0.6$  eV, see Figure 3.2). An analysis based on statistical hypothesis testing and the sum of the individual differences between the AIMD and AIMDf results divided by the standard errors in these differences shows that, for the two rovibrational states addressed and the collision energies for which reasonably accurate AIMD results could be obtained, the AIMD results fall below the AIMDf results on average (significance level  $\alpha = 0.05$ , see Appendix 3.A.1). Modeling surface motion with AIMD also leads to a clear and statistically significant improvement in the overall agreement with experiment when comparing to the AIMDf results and the previous quantum dynamical and quasi-classical BOSS results [10, 11] (see Appendix 3.A.1). On average, the AIMDf alignment parameters are significantly lower, and therefore in better agreement with experiment than the previous QCT-BOSS results (see Appendix 3.A.1), which we attribute to improvements in the static surface model achieved here through the AIMDf calculations as already discussed in Section 3.2. Finally, we note that the similarity between the quantum dynamical and QCT-BOSS results in Figure 3.2 validates the use of quasi-classical mechanics in AIMD to compute  $A_0^{(2)}$ .

In Figure 3.3 the AIMD results for  $R_{v,J}(E)$  are in much better agreement with experimentally fitted [15,30] results for the  $(v = 0, J = 11)$  state at  $T_s = 925$  K than the previous QCT-BOSS model results with experimentally fitted [15,30] results for  $T_s = 120$  K [10,11], for the lower  $E$  for which the experimental fits can be expected to be most reliable. The improvement may well be due in large part to improvements introduced in AIMD other than allowing surface motion (see also Section 3.2), as the difference between the AIMD and AIMDf results is smaller than between AIMD and QCT-BOSS. The AIMD value of the energy  $E_0$  ( $0.574 \pm 0.009$  eV) at which the reaction probability becomes equal to half the maximum experimentally fitted value ( $A = 0.27$  [30]) agrees with the experimental value (0.546 eV) to within chemical accuracy (1 kcal/mol  $\approx$  43 meV). AIMD calculations for additional rovibrational states are needed to establish whether the AIMD method can describe the experimental  $E_0(v, J)$  values for  $D_2$  with chemical accuracy for the greater part of the  $(v, J)$  states for which experimental results

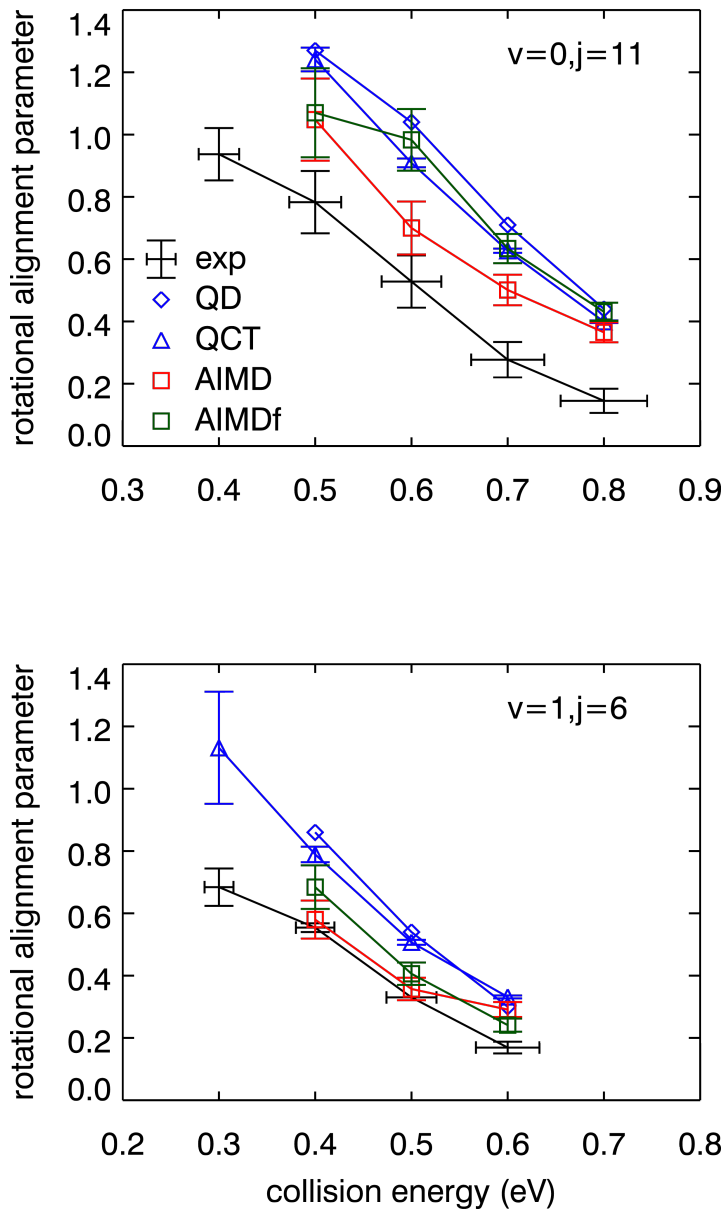


Figure 3.2: Comparison of  $A_0^{(2)}$  values measured in associative desorption experiments [3] with theoretical values computed using the AIMD method, the AIMD method with the surface held fixed at 0 K (AIMDf), and with quantum dynamics (QD) and the QCT method using the BOSS model [10, 11].

are available (see also Chapter 4); only marginal improvement was observed for ( $v = 1, J = 6$ ) here (Figure 3.3, the difference between the AIMD and experimental  $E_0$  values is 45 meV). The comparison of the AIMD and AIMDf results is consistent with the finding of low-dimensional calculations using surface oscillator approximations [13, 17] and experiments [15, 31] that raising  $T_s$  broadens the reaction probability around a common midpoint.

The fact that  $A_0^{(2)}$  may be written as a fraction (Equation 3.1) suggests the existence of two distinguishable mechanisms that may lead to a decrease of this parameter. Figure 3.4 illustrates these two mechanisms, for the ( $v = 1, J = 6$ ) state. At the lowest  $E$  the denominator of the fraction increases because  $R_{v,J}(E)$  increases with  $T_s$  (see also Figure 3.3), leading to a decrease in  $A_0^{(2)}$  (Figure 3.2) even though cartwheel (low  $|m_J|$ ) reaction probabilities do not increase more than helicopter (high  $|m_J|$ ) reaction probabilities, leaving the numerator in Equation 3.1 almost unchanged (mechanism I, see Appendix 3.A.2). The importance of this mechanism at low  $E$  is consistent with DFT findings that the molecule-surface interaction is decreased in an isotropic fashion for the two lowest high symmetry barrier geometries (bridge-to-hollow and the t2h site halfway between a top and hcp site) if the closest second layer (or hcp) Cu atom moves down (see Figure 9 of Ref. [20]). Such configurations will be increasingly available at high  $T_s$ . At these configurations the energy available to reaction (the molecule’s energy minus the height of the barrier) is increased, whereas the ‘anisotropy energy’ (which may be defined as the interaction energy of a tilted molecule minus that of a parallel molecule at the reaction barrier geometry [3]) is unchanged. Under these conditions, the reaction probability may be expected to increase by the same amount for all  $m_J$  (as seen in Figure 3.4 for 0.4 eV), which is consistent with the mechanism discussed above. A reasoning based on increasing available energy and unchanged anisotropy energy has also been invoked to explain the dependence of  $A_0^{(2)}$  on incidence energy [3].

Figure 3.4 shows that at the intermediate  $E$  of 0.5 eV the decrease in  $A_0^{(2)}$  (Figure 3.2) is due to increased reaction of states with low  $|m_J|$  and decreased reaction of states with high  $|m_J|$ , leading to a decrease in the numerator of Equation 3.1 whereas the

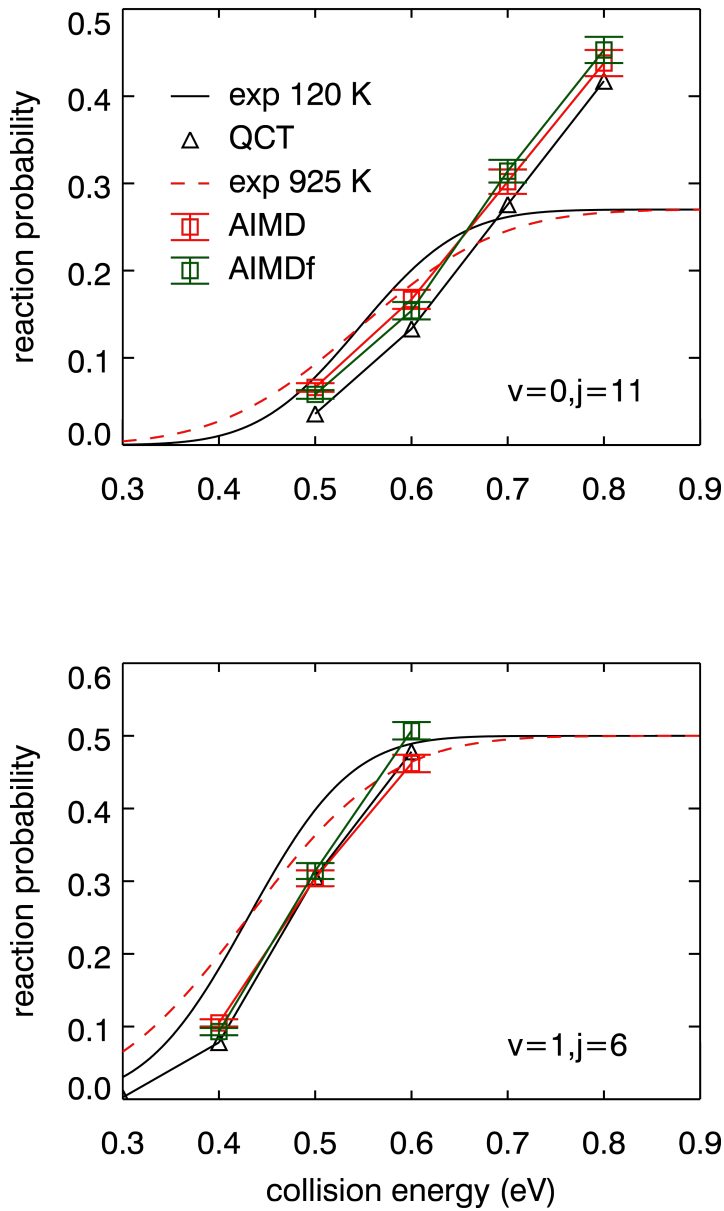


Figure 3.3: Comparison of experimentally fitted [15,30] values of  $R_{v,j}(E)$  for  $T_s = 120$  and 925 K with theoretical values computed using the AIMD and AIMDf methods and with the QCT method using the BOSS model [10,11].

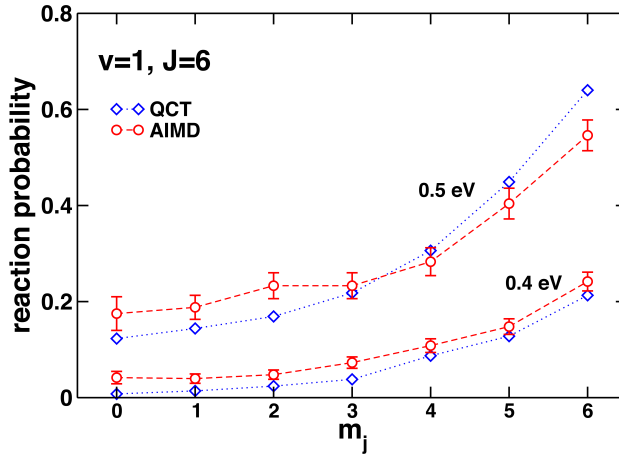


Figure 3.4: Comparison of  $R_{v,J,m_J}(E)$  computed with AIMD with QCT results using the BOSS model [10, 11] for  $(v = 1, J = 6)$   $D_2 + Cu(111)$ .

denominator is almost unchanged (it is actually decreased see Appendix 3.A.2), in what we call mechanism II. The above two cases represent ideal cases: in some cases a change in  $A_0^{(2)}$  reflects both changes in the preference for helicopter vs. cartwheel reaction and changes in  $R_{v,J}(E)$ . We have also seen cases where changes in the numerator and the denominator work in opposite ways but one of the effect dominates, see Appendix 3.A.2. Our interpretation of mechanism II is as follows. On a cold surface, the preference found for reaction with  $D_2$  parallel to the surface arises from the barrier being lowest in this alignment, because it best allows the D-atoms to simultaneously form bonds to the surface. On a hot surface the preference for parallel reaction is diminished because the molecule is more likely to encounter environments in which the surface is locally distorted, such that the simultaneous formation of D-metal bonds may be favored for tilted configurations. One would then expect increased reaction of states with low  $|m_J|$  and decreased reaction of states with high  $|m_J|$ , whereas  $R_{v,J}(E)$  might remain unchanged.

The increase in  $R_{v,J}(E)$  in mechanism I is not only correlated with motion of the second layer Cu atom closest to the impinging  $D_2$  molecule, but also to motion of the closest first layer Cu atom, because the barrier height is decreased for the lowest

D <sub>2</sub> state	$E$ (eV)	$Z_{12}^{av}$ , reaction	$Z_{12}^{av}$ , scattering
$v = 1, J = 6$	0.4	$2.273 \pm 0.012$	$2.194 \pm 0.004$
$v = 0, J = 11$	0.5	$2.292 \pm 0.022$	$2.196 \pm 0.005$
$v = 0, J = 11$	0.6	$2.260 \pm 0.019$	$2.182 \pm 0.008$

Table 3.1: The average value of  $Z_{12}$  (in Å) and its error is shown for reacting D<sub>2</sub> (computed when  $r$  first becomes larger than 1.032 Å, the value at the SRP minimum reaction barrier geometry [10]) and for scattering D<sub>2</sub> (computed at the largest outer turning point in  $r$  of scattering D<sub>2</sub>).

reaction barrier geometry if this Cu atom moves up [20]. Indeed, in reactive events, and for the initial states and energies at which mechanism I operates or an increase in  $R_{v,J}(E)$  contributes to a decreased alignment parameter (Appendix 3.A.2), we observe significantly larger values  $Z_{12}$  of the vertical distance between these Cu-atoms than for scattering (Table 3.1). At the  $T_s$  considered here large  $Z_{12}$  values do not only result from large amplitude phonon motion, but also from thermal expansion: experiments show that the first interlayer distance  $d_{12}$  goes up by 2.7% going from 0 to 925 K. The large increase of  $d_{12}$  reflects both thermal expansion of the bulk (1.54% [27, 28]) and  $d_{12}$  being contracted with respect to the bulk at low  $T_s$ , but bulk-like at high  $T_s$  [32]. Our DFT and AIMD calculations reproduce this trend: The average  $d_{12}$  obtained with AIMD for  $T_s = 925$  K ( $2.189 \pm 0.034$  Å) is larger than the  $d_{12}$  value that characterizes a (0 K) relaxed slab (2.10 Å, see Table 3.2) and agrees, within error bars, with the bulk interlayer distance of 2.16 Å expected for the (expanded) lattice constant of 3.74 Å. The lowering of the barrier heights we see (Table 3.2) with increased tensile strain ( $T_s$ ) may be explained [33] from the d-band model [34]: smaller overlap between substrate atoms reduces the width of the d-band, causing an upshift of the band if it is more than half-filled, which usually leads to higher reactivity.

The error bars on the experimental results in Figure 3.2 are estimates of confidence intervals based on an assessment of systematic errors that affect the energy calibration and limited information on statistical errors: They were based on noise in the time-of-flight spectra and uncertainties in the fits used, but on only one set (two sets) of measurements for  $v = 1, J = 6$  ( $v = 0, J = 11$ ) [35]. Conversely, the AIMD error bars only represent statistical errors. In the AIMD, systematic errors can arise from the use

Parameter	925 K	0 K
$d_{12}$ (Å)	2.16	2.10
$a_{3D}$ (Å)	3.74	3.68
$E_b$ (bth)	0.593	0.628
$E_b$ (ttb)	0.865	0.877

Table 3.2: Parameters describing slab geometry and molecule-surface interaction energies ( $E_b$ , in eV) obtained with DFT and the SRP48 functional are presented for the bridge-to-hollow (bth) and top-to-bridge (ttb) dissociation routes at SRP reaction barrier geometries [10], for  $T_s = 0$  and 925 K.

of too few Cu layers or a too small surface unit cell to adequately model surface motion. Considering the uncertainties in the experimental and theoretical error analyses, we argue that the best statement we can make presently about the agreement with experiment is that going from the BOSS model to the AIMD model, which allows the surface to move, the overall agreement is improved significantly. We believe that further theoretical work aimed at eliminating the systematic errors that may still be present in the AIMD is best performed when experimental results accompanied by a more complete error analysis become available. If the differences between theory based on the detailed balance assumption and associative desorption experiments persist, further research should be performed to address the validity of this assumption. For instance, it is possible that the permeation technique leads to an overestimated contribution of reaction involving D-atoms coming directly from the subsurface, which may be investigated with additional calculations, or using alternative techniques to dose D-atoms to the surface [31].

### 3.4 Summary and Conclusions

We have employed the AIMD method to study the effect of surface temperature on the rotational quadrupole alignment parameter for  $D_2$  desorbing from Cu(111). We have investigated the two molecular rovibrational states for which experimental data [3] are available at various collision energies, basing our model on the assumption of detailed balance. Our calculations show that the alignment parameter is on average lowered when the high experimental surface temperature (925 K) is modeled, improving in this way the agreement with the experiment. We suggest two mechanisms to explain the



decrease of the rotational alignment parameter with increased surface temperature. The first mechanism is related to an increased reactivity for all the molecular alignments: the impinging molecules experience lower dissociation barriers because of the larger vertical distance between the closest first layer atom and second layer atom sampled at high surface temperature. The second mechanism, on the other hand, has to do with a diminished reactivity of the molecular orientations with the bond parallel to the surface and an increased reactivity of the tilted orientations, provoked by local surface deformations, also frequently sampled at high surface temperature. The mismatch still present between theory and experiment in the alignment parameter could be due to systematic errors in the AIMD method or to an incomplete error analysis of the experimental data. For what concerns the initial-state-selected reaction probability, only slight improvement is observed against previous static surface calculations, with AIMD curves being slightly broader than AIMDf curves. This increase of the width is in agreement with previous theoretical [13,17] and experimental [15,31] findings about the effect of surface temperature on the shape of the dissociation probability curves, but the size of the increase is too small when compared with experimental findings [15,31].

## 3.A Appendix

### 3.A.1 Statistical Analysis

In this section we aim to show that the rotational quadrupole alignment parameters obtained with AIMD are smaller than the AIMDf values obtained for a 0 K static surface. Such a proof can be put on a firm statistical basis by using the method of statistical hypothesis testing [36]. We will concern ourselves with differences  $d_i$  divided by the standard error  $s_i$  in these differences, or by the standard deviation  $\sigma_i$  in these differences, for combinations of translational energies and  $(v, J)$   $D_2$  states denoted by  $i$ . The difference may be between any two sets of measurements, but in the example considered here first it concerns the AIMD and the AIMDf calculations of the alignment parameter. For this case,  $d_i$  is defined by:

$$d_i = A_0^{(2)}(J; \text{AIMDf}, i) - A_0^{(2)}(J; \text{AIMD}, i). \quad (3.A.1)$$

In hypothesis testing, we take the hypothesis we try to prove as the alternative hypothesis, which we may write as:

- $H_1$ : Modeling the effect of surface temperature decreases the rotational quadrupole alignment parameter. The AIMD results should therefore fall below the AIMDf results, and the differences defined in Equation 3.A.1 should be positive.

Next, we formulate the null hypothesis, which can be taken opposite to the hypothesis we are trying to prove, as:

- $H_0$ : Modeling the effect of surface temperature does not affect the rotational quadrupole alignment parameter, or increases it. The AIMDf results should therefore fall below or on the AIMD results, and the differences defined in Equation 3.A.1 should be zero or negative.

In order to be able to accept the  $H_1$  hypothesis posed, in statistical hypothesis testing one then demands that, on the basis of the data obtained,  $H_0$  can be rejected with a pre-defined confidence level  $\alpha$ , which imposes a maximum on the probability to reject

#	State	$E$ (eV)	$d_i$	$\sigma_i$	$Z$ -statistic	$p$ -value
1	$(v = 1, J = 6)$	0.4	0.10342	0.09298	1.1123	0.1335
2	$(v = 1, J = 6)$	0.5	0.04986	0.05092	0.9792	0.1635
3	$(v = 1, J = 6)$	0.6	-0.04941	0.03178	-1.5548	N/A
4	$(v = 0, J = 11)$	0.5	0.02161	0.19466	0.1110	0.4562
5	$(v = 0, J = 11)$	0.6	0.28366	0.13105	2.1645	0.0152
6	$(v = 0, J = 11)$	0.7	0.13286	0.06751	1.9680	0.0244
7	$(v = 0, J = 11)$	0.8	0.06643	0.04335	1.5324	0.0630

Table 3.A.1:  $Z$ -statistics and  $p$ -values for 7 computational experiments, comparing AIMDf with AIMD results.

$H_0$  if  $H_0$  is true. A typical value used for  $\alpha$  is 0.05 and this is the value we will work with. One next calculates the actual probability of rejecting  $H_0$  although  $H_0$  is true, in the light of the data obtained. This probability is called the  $p$ -value, which should be lower than  $\alpha$  for  $H_0$  to be rejected. Assuming for now that the calculated standard error in the difference,  $s_i$ , equals the standard deviation in the difference,  $\sigma_i$ , we base our test on the so-called  $Z$ -statistic or  $Z$ -score, which for the condition  $i$  may be written as [36]:

$$Z_i = \frac{d_i}{\sigma_i}. \quad (3.A.2)$$

Table 3.A.1 lists the  $Z$ -statistics for our seven computational experiments, and the  $p$ -values for rejecting  $H_0$  on the basis of an individual measurement. The Table shows a drawback of the AIMD method, which is computationally expensive. As a result, the computed alignment parameters are based on reaction probabilities calculated from a limited number of trajectories. The statistical errors in these probabilities are inversely proportional to the square root of the number of trajectories, and these errors are therefore rather large. This results in rather large statistical errors in the alignment parameters and their differences  $d_i$ . As a result, in only two of the 7 individual cases the  $Z$ -statistics are large enough, and the  $p$ -values small enough to allow rejection of the null hypothesis for the specific condition investigated.

However, six of the seven  $Z$ -statistics are positive, pointing to the fact that a much stronger statement is possible if the measurements are considered together. We reformulate our hypotheses as follows:

- $H_1$ : On average, for the two rovibrational states for which energy resolved measurements are available and the ranges of collision energies for which statistically accurate alignment parameters could be obtained, modeling surface temperature decreases the rotational quadrupole alignment parameter. On average, the AIMD results should therefore fall below the AIMDf results.
- $H_0$ : On average, for the two rovibrational states for which energy resolved measurements are available and the ranges of collision energies for which statistically accurate alignment parameters could be obtained, modeling surface temperature does not affect the rotational quadrupole alignment parameter, or increases it. On average, the AIMDf results should therefore fall below or on the AIMD results.

We can test these hypotheses using the sum of the individual  $Z$ -scores. This weighs each measurement according to the error in it, and we obtain a test-statistic which is guaranteed to have a normal distribution, provided that the individual  $Z$ -scores also obey a normal distribution, which we assume to be the case anyway.

The individual  $Z$ -statistics obey the normal distribution  $N(0, 1)$ , 0 being the average and 1 the variance. It is easy to see that  $\sum_{i=1}^7 Z_i$  obeys the normal distribution  $N(0, 7)$ . We may then obtain a composite  $Z$ -statistic by defining:

$$Z_{comp} = \frac{\sum_{i=1}^7 Z_i}{\sqrt{7}} \quad (3.A.3)$$

(this composite  $Z$ -score is also known as Stouffer's  $Z$ -score [37]). From the data in Table 3.A.1 we obtain  $Z_{comp} = 2.38$ . The  $H_0$  hypothesis may be formulated as  $Z_{comp} \leq 0$ . The  $p$ -value of the outcome  $Z_{comp} = 2.38$  is 0.0085. Clearly, the null hypothesis may be rejected with a significance level of 0.05, and we may accept our new  $H_1$  hypothesis which concerns the ensemble of initial conditions we have AIMD results for.

In a similar way, we may test the alternative hypothesis that, on average, for the two rovibrational states for which energy resolved measurements are available and the ranges of collision energies for which statistically accurate alignment parameters could be obtained, the AIMD method modeling the effect of  $T_s$  yields results in better agreement

with experiment than the AIMDf method. This requires the sum of the absolute values of the differences between the experimental results and the AIMD results to be smaller than the sum of the absolute values of the differences between the experimental results and the AIMDf results. Because in all cases  $i$  the experimental  $A_0^{(2)}(J)$  values are lower than both the AIMD values of  $A_0^{(2)}(J)$  and the AIMDf values of  $A_0^{(2)}(J)$ , this amounts to proving that on average, modeling surface temperature with AIMD decreases the rotational quadrupole alignment parameter. This was already done above, and we can reject the null hypothesis that, on average, modeling surface temperature with AIMD does not yield increased agreement with experiment with a confidence level  $\alpha=0.05$  and with the same  $p$ -value as obtained before (0.0085).

In a similar vein, we are able to prove that, on average, the fixed surface model implicit in the AIMDf calculations improves the agreement with experiment compared to the fixed surface model used in the previous QCT-BOSS calculations [10, 11], due to the improvements discussed above ( $p$ -value of 0.003). Finally, the improved agreement with experiment going from the QCT-BOSS fixed surface model to the AIMDf fixed surface model and then to the AIMD model with  $T_s = 925$  K can also be seen simply by comparing the sum of the absolute differences:

$$S = \sum_{i=1}^7 |d_i|, \quad (3.A.4)$$

with:

$$d_i = A_0^{(2)}(J; \text{exp}, i) - A_0^{(2)}(J; \text{method}, i). \quad (3.A.5)$$

The results are presented in Table 3.A.2. If we take  $S$  as a measure of the disagreement with experiment, going from the AIMDf model to the AIMD model the disagreement with experiment is reduced by almost a factor 1.6. Going from the previous QCT-BOSS static surface results to the AIMD results modeling surface motion, the disagreement with experiment is reduced by almost a factor 2.

Model	$S$
QCT-BOSS	2.02
AIMDf	1.66
AIMD	1.06

Table 3.A.2: The sum of the absolute differences with the experimental alignment parameter values,  $S$ , is given for the alignment parameters computed with the AIMD, the AIMDf, and the QCT-BOSS models.

### 3.A.2 Relative Importance of the Two Mechanisms for Reducing the Alignment Parameter

The fractional decrease of the AIMD alignment parameter due to surface motion may be written as:

$$\frac{A_0^{(2)}(J; \text{AIMDf}) - A_0^{(2)}(J; \text{AIMD})}{A_0^{(2)}(J; \text{AIMDf})} = (1 - A_{fac}) + (1 - B_{fac}) - (1 - A_{fac})(1 - B_{fac}), \quad (3.A.6)$$

with:

$$A_{fac} = A_{\text{AIMD}}/A_{\text{AIMDf}}, \quad (3.A.7a)$$

$$B_{fac} = B_{\text{AIMD}}/B_{\text{AIMDf}}. \quad (3.A.7b)$$

and where A and B are defined in Equation 3.1 in Section 3.2. The last term on the rhs of Equation 3.A.6 is small and, for ease of interpretation in terms of the contribution of mechanisms I and II to the decrease of the alignment parameter, we may ignore it (it hardly affects the contributions discussed below). We therefore write:

$$\frac{A_0^{(2)}(J; \text{AIMDf}) - A_0^{(2)}(J; \text{AIMD})}{A_0^{(2)}(J; \text{AIMDf})} = (1 - A_{fac}) + (1 - B_{fac}). \quad (3.A.8)$$

On the basis of Equation 3.A.8 the fractional decrease may be analyzed in terms of two fractional contributions to the decrease of the alignment parameter, one being due to mechanism I:

$$C_I = \frac{1 - B_{fac}}{(1 - A_{fac}) + (1 - B_{fac})}, \quad (3.A.9)$$

#	State	$E$ (eV)	$C_I$	$C_{II}$
1	$(v = 1, J = 6)$	0.4	0.69	0.31
2	$(v = 1, J = 6)$	0.5	$< 0$	$> 1$
3	$(v = 1, J = 6)$	0.6	N/A	N/A
4	$(v = 0, J = 11)$	0.5	$> 1$	$< 0$
5	$(v = 0, J = 11)$	0.6	0.26	0.74
6	$(v = 0, J = 11)$	0.7	$< 0$	$> 1$
7	$(v = 0, J = 11)$	0.8	$< 0$	$> 1$

Table 3.A.3: The fractional contributions of the two mechanisms to the decrease of the alignment parameter with  $T_s$  computed with the AIMD method is shown for the seven initial conditions investigated in the calculations.

and one being due to mechanism II:

$$C_{II} = \frac{1 - A_{fac}}{(1 - A_{fac}) + (1 - B_{fac})}. \quad (3.A.10)$$

With the approximation made in Equation 3.A.8, these coefficients add up to 1. Their interpretation is that if  $C_I > C_{II}$  mechanism I makes a dominant contribution to the decrease of the alignment parameter, whereas mechanism II makes the dominant contribution if  $C_I < C_{II}$ .

The fractional contributions are given in Table 3.A.3 for the 7 initial conditions considered here. Mechanism I is most important for the lowest incidence energy for both initial rovibrational states and makes a considerable contribution for  $(v = 0, J = 11)$  at  $E = 0.6$  eV. It is precisely for these three conditions that, in a statistically significant way, we can correlate reaction with a collective motion of the Cu atoms that are in the upper two surface layers and closest to the reacting D<sub>2</sub>, which motion results in an isotropic decrease of the reaction barrier height at the lowest reaction barrier geometry (see Section 3.3 and Table 3.1). For the higher incidence energies, mechanism II dominates.

## Bibliography

- [1] B. L. Yoder, R. Bisson, and R. D. Beck, *Science* **329**, 553 (2010).
- [2] M. Rutkowski, D. Wetzig, and H. Zacharias, *Phys. Rev. Lett.* **87**, 246101 (2001).
- [3] H. Hou, S. J. Gulding, C. T. Rettner, A. M. Wodtke, and D. J. Auerbach, *Science* **277**, 80 (1997).
- [4] M. Rutkowski and H. Zacharias, *Phys. Chem. Chem. Phys.* **3**, 3645 (2001).
- [5] D. A. McCormack, G. J. Kroes, R. A. Olsen, J. A. Groeneveld, J. N. P. van Stralen, E. J. Baerends, and R. C. Mowrey, *Chem. Phys. Lett.* **328**, 317 (2000).
- [6] I. Chorkendorff and J. W. Niemantsverdriet, *Concepts of Modern Catalysis and Kinetics*, Wiley-VCH, Weinheim, 2003.
- [7] R. Peverati and D. G. Truhlar, *Phys. Chem. Chem. Phys.* **14**, 13171 (2012).
- [8] R. Peverati and D. G. Truhlar, *Phil. Trans. R. Soc. A* **372**, 20120476 (2014).
- [9] A. Dianat and A. Groß, *Phys. Chem. Chem. Phys.* **4**, 4126 (2002).
- [10] C. Díaz, E. Pijper, R. A. Olsen, H. F. Busnengo, D. J. Auerbach, and G. J. Kroes, *Science* **326**, 832 (2009).
- [11] C. Díaz, R. A. Olsen, D. J. Auerbach, and G. J. Kroes, *Phys. Chem. Chem. Phys.* **12**, 6499 (2010).
- [12] P. Nieto, E. Pijper, D. Barredo, G. Laurent, R. A. Olsen, E. J. Baerends, G. J. Kroes, and D. Fariás, *Science* **312**, 86 (2006).
- [13] M. Dohle and P. Saalfrank, *Surf. Sci.* **373**, 95 (1997).
- [14] Y. Y. Chuang, M. L. Radhakrishnan, P. L. Fast, C. J. Cramer, and D. G. Truhlar, *J. Phys. Chem. A* **103**, 4893 (1999).
- [15] H. A. Michelsen, C. T. Rettner, D. J. Auerbach, and R. N. Zare, *J. Chem. Phys.* **98**, 8294 (1993).
- [16] Z. S. Wang, G. R. Darling, B. Jackson, and S. Holloway, *J. Phys. Chem. B* **106**, 8422 (2002).
- [17] Z. S. Wang, G. R. Darling, and S. Holloway, *J. Chem. Phys.* **120**, 2923 (2004).
- [18] H. F. Busnengo, W. Dong, and A. Salin, *Phys. Rev. Lett.* **93**, 236103 (2004).
- [19] H. F. Busnengo, M. A. Di Césare, W. Dong, and A. Salin, *Phys. Rev. B* **72**, 125411 (2005).
- [20] M. Bonfanti, C. Díaz, M. F. Somers, and G. J. Kroes, *Phys. Chem. Chem. Phys.* **13**, 4552 (2011).
- [21] A. Groß and A. Dianat, *Phys. Rev. Lett.* **98**, 206107 (2007).
- [22] G. Kresse and J. Hafner, *Phys. Rev. B* **47**, 558 (1993).



- [23] G. Kresse and J. Hafner, Phys. Rev. B **49**, 14251 (1994).
- [24] G. Kresse and J. Furthmüller, Comput. Mat. Sci. **6**, 15 (1996).
- [25] G. Kresse and J. Furthmüller, Phys. Rev. B **54**, 11169 (1996).
- [26] G. Kresse and D. Joubert, Phys. Rev. B **59**, 1758 (1999).
- [27] F. R. Kroeger and C. A. Swenson, J. Appl. Phys. **48**, 853 (1977).
- [28] I. E. Leksina and S. I. Novikova, Sov. Phys-Solid State **5**, 798 (1963).
- [29] J. P. Perdew, K. Burke, and M. Ernzerhof, Phys. Rev. Lett. **77**, 3865 (1996).
- [30] C. T. Rettner, H. A. Michelsen, and D. J. Auerbach, Faraday Discuss. **96**, 17 (1993).
- [31] M. J. Murphy and A. Hodgson, J. Chem. Phys. **108**, 4199 (1998).
- [32] K. H. Chae, H. C. Lu, and T. Gustafsson, Phys. Rev. B **54**, 14082 (1996).
- [33] S. Sakong and A. Groß, Surf. Sci. **525**, 107 (2003).
- [34] B. Hammer and J. K. Nørskov, Surf. Sci. **343**, 211 (1995).
- [35] D. J. Auerbach and A. M. Wodtke, Private Communication, 2012.
- [36] W. L. Hayes, *Statistics*, Holt, Rinehart and Winston, NY, 3rd edition, 1981.
- [37] S. A. Stouffer, E. A. Suchman, L. C. De Vinney, S. A. Star, and R. M. Williams Jr., *The American Soldier: Adjustment During Army Life (Vol. 1)*, Princeton University Press, Princeton, 1949.

